

RESEARCH ARTICLE

Trade-off and flexibility in the dynamic regulation of the cullin-RING ubiquitin ligase repertoire

Ronny Straube^{1*}, Meera Shah², Dietrich Flockerzi^{1,3}, Dieter A. Wolf^{2,4*}

1 Max Planck Institute for Dynamics of Complex Technical Systems Magdeburg, Magdeburg, Germany, **2** Sanford Burnham Prebys Medical Discovery Institute, La Jolla, California, United States of America, **3** Institute for Automation Engineering, Otto-von-Guericke University Magdeburg, Magdeburg, Germany, **4** School of Pharmaceutical Sciences, Xiamen University, Xiamen, Fujian, China

* rstraube@mpi-magdeburg.mpg.de (RS); [dewolf@sbpdiscovery.org](mailto:dwolf@sbpdiscovery.org) (DAW)



OPEN ACCESS

Citation: Straube R, Shah M, Flockerzi D, Wolf DA (2017) Trade-off and flexibility in the dynamic regulation of the cullin-RING ubiquitin ligase repertoire. *PLoS Comput Biol* 13(11): e1005869. <https://doi.org/10.1371/journal.pcbi.1005869>

Editor: Vahid Shahrezaei, Imperial College London, UNITED KINGDOM

Received: February 27, 2017

Accepted: November 2, 2017

Published: November 17, 2017

Copyright: © 2017 Straube et al. This is an open access article distributed under the terms of the [Creative Commons Attribution License](https://creativecommons.org/licenses/by/4.0/), which permits unrestricted use, distribution, and reproduction in any medium, provided the original author and source are credited.

Data Availability Statement: All relevant data are within the paper and its Supporting Information files.

Funding: Work in DAW's lab was funded by grants GM105802 and GM121834 from the US National Institutes of Health, the Foreign 1000 Talent Program of the Government of the People's Republic of China, and the 100 Talent Program of the Province of Fujian, China. The funders had no role in study design, data collection and analysis, decision to publish, or preparation of the manuscript.

Abstract

Cullin-RING ubiquitin ligases (CRLs) catalyze the ubiquitylation of substrates many of which are degraded by the 26S proteasome. Their modular architecture enables recognition of numerous substrates via exchangeable substrate receptors that competitively bind to a cullin scaffold with high affinity. Due to the plasticity of these interactions there is ongoing uncertainty how cells maintain a flexible CRL repertoire in view of changing substrate loads. Based on a series of *in vivo* and *in vitro* studies, different groups proposed that the exchange of substrate receptors is mediated by a protein exchange factor named Cand1. Here, we have performed mathematical modeling to provide a quantitative underpinning of this hypothesis. First we show that the exchange activity of Cand1 necessarily leads to a trade-off between high ligase activity and fast receptor exchange. Supported by measurements we argue that this trade-off yields an optimal Cand1 concentration in cells where the time scale for substrate degradation becomes minimal. In a second step we show through simulations that (i) substrates bias the CRL repertoire leading to preferential assembly of ligases for which substrates are available and (ii) differences in binding affinities or substrate receptor abundances create a temporal hierarchy for the degradation of substrates. Finally, we compare the Cand1-mediated exchange cycle with an alternative architecture lacking Cand1 which indicates superiority of a system with exchange factor if substrate receptors bind substrates and the cullin scaffold in a random order. Together, our results provide general constraints for the operating regimes of molecular exchange systems and suggest that Cand1 endows the CRL network with the properties of an “on demand” system allowing cells to dynamically adjust their CRL repertoire to fluctuating substrate abundances.

Author summary

Cullin-RING ubiquitin ligases (CRLs) are multisubunit protein complexes where exchangeable substrate receptors (SRs) assemble on a cullin scaffold to mediate ubiquitylation and subsequent degradation of a large variety of substrates. In humans there are

Competing interests: The authors have declared that no competing interests exist.

hundreds of different CRLs having potentially thousands of substrates. Due to the high affinity of cullin-SR interactions, it has long been a mystery how cells would maintain flexibility to sample the entire SR repertoire in order to match fluctuating substrate loads. Recent experiments indicate that the exchange of different SRs is mediated by a novel protein exchange factor (Cand1). However, the proposed biochemical function of Cand1 as a promoter of CRL activity remained difficult to reconcile with previous reports of Cand1 acting as an inhibitor of CRL activity *in vitro*. Here we show that these two findings are not contradictory, but that the exchange activity of Cand1 necessarily leads to a trade-off between high ligase activity and fast receptor exchange which leads us to predict an optimal Cand1 concentration and a temporal hierarchy for substrate degradation. Our results support the view that Cand1 endows the CRL network with the flexibility of an “on demand” system where relative CRL abundances are dictated by substrate availability.

Introduction

Cullin-RING ubiquitin ligases (CRLs) are modular protein assemblies that target cellular substrates for ubiquitylation, a modification which may alter the activity of a substrate or lead to its degradation by the 26S proteasome [1, 2]. CRLs have been implicated in the regulation of numerous cellular processes which makes them attractive targets for the development of drugs [3–5]. The class of SCF (Skp1-Cul1-F-box) ubiquitin ligases represents the defining member of the CRL family [6, 7]. SCF ligases consist of a cullin1 (Cul1) scaffold (Fig 1A) with the RING finger protein Rbx1 (RING-box protein 1) bound to its C-terminal domain [8]. The latter acts as a binding site for an associated ubiquitin-conjugating enzyme (E2). Substrates to be ubiquitylated are recognized by dedicated F-box containing substrate receptors which bind to the N-terminal region of Cul1 via the Skp1 adapter protein. There are potentially 69 SCF complexes in humans. Since their total concentration exceeds that of the cullin scaffold [9] access of free SRs to Cul1 is under competition. Also, Cul1-SR binding appears to be extraordinarily tight [10] making spontaneous dissociation of preformed SCF complexes extremely unlikely and raising the question how access of different SRs to Cul1 is regulated in cells.

SCF ligases are activated through covalent attachment of the ubiquitin-like protein Nedd8 to Cul1. Nedd8 attachment has multiple effects on SCF activity: It recruits a priming E3 ligase [11], increases the binding affinity of Rbx1 for ubiquitin-loaded E2 enzyme (E2-Ub) [12, 13] and positions the latter in close proximity to the substrate [14]. In the absence of substrate Nedd8 is removed from Cul1 by the COP9 signalosome (CSN) [9, 15, 16]. Interestingly, when Cul1 is not neddylated SRs can be removed from Cul1 by cullin-associated and neddylation-dissociated 1 (Cand1) which acts as an exchange factor for SRs [10, 17, 18]. Binding of Cand1 to a SCF complex dramatically increases the SR dissociation rate constant (10^6 -fold) in a manner that is similar to nucleotide exchange factors when catalyzing the exchange of GDP for GTP in small GTPases [19], i.e. through formation of a short-lived ternary complex (Fig 1B). Based on genetic evidence it has been argued that the exchange activity of Cand1 is required for efficient substrate degradation *in vivo* [20–23] and that Cand1 may potentially bias the assembly of SCF complexes towards F-box proteins for which substrates are available [10, 24]. However, when analyzed *in vitro* Cand1 has been found to act as an inhibitor of SCF ligase activity [13, 20, 25–28]. In the present study we used mathematical modeling and analysis of Cand1-mediated SR exchange to address this apparent paradox. Our results suggest that previous *in vivo* and *in vitro* findings are not contradictory, but that the exchange activity of Cand1 necessarily generates a trade-off between high SCF occupancy and fast SR exchange. This

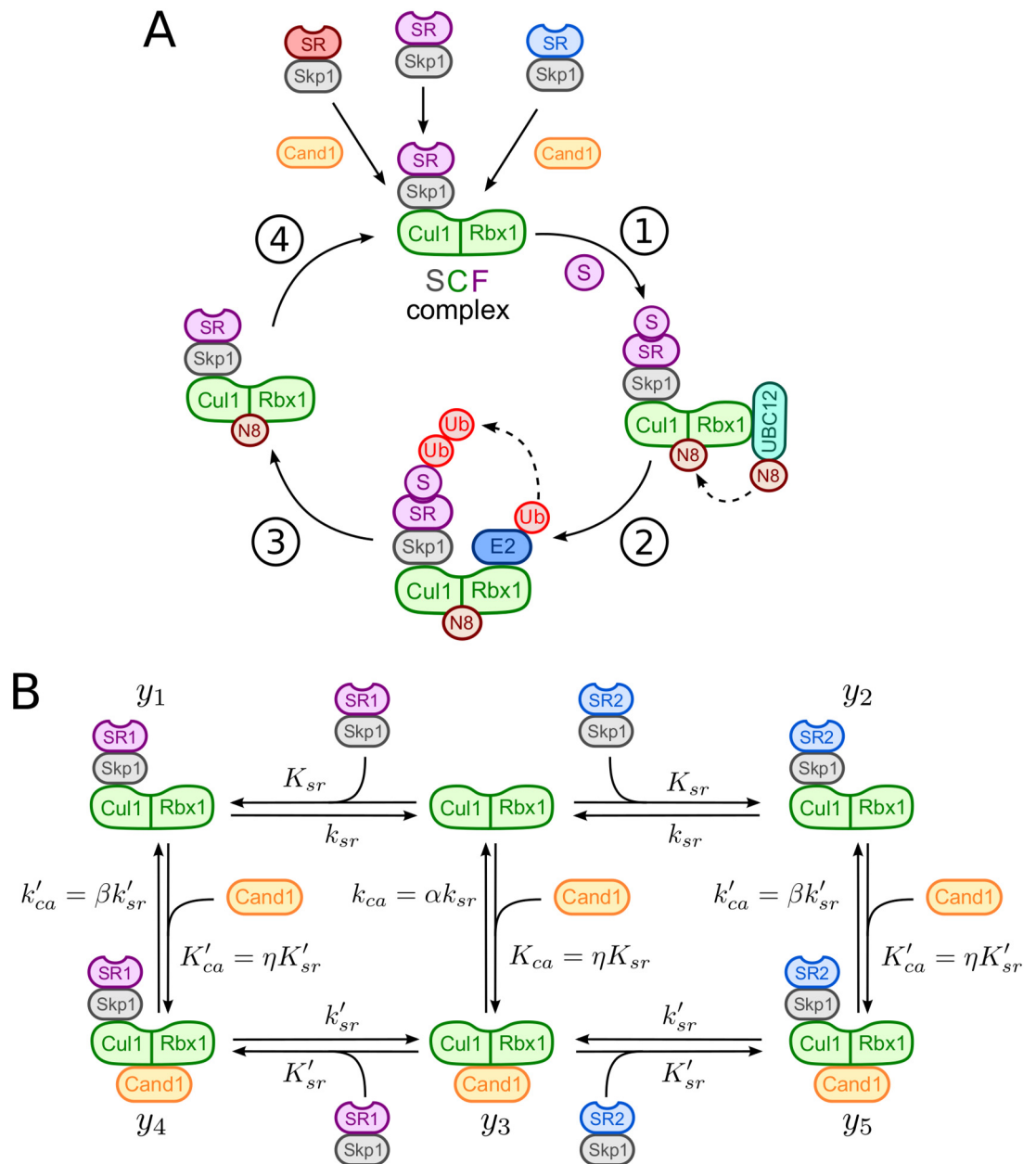


Fig 1. SCF-mediated substrate degradation and Cand1 cycle. **A:** Scheme of SCF-mediated substrate degradation: (1) Substrate (S) binding to substrate receptors (Skp1/SR) and UBC12-mediated neddylation (N8) of Cul1, (2) E2 recruitment, ubiquitin (Ub) transfer by E2 to the substrate and Ub chain elongation, (3) substrate degradation by the 26S proteasome and (4) deneddylation of Cul1 by the COP9 signalosome. Relative sizes of protein subunits are not to scale. **B:** Model of the Cand1-mediated exchange cycle for two substrate receptors (Skp1/SR1 and Skp1/SR2). K_{sr} , K_{ca} , K'_{sr} and K'_{ca} denote dissociation constants whereas k_{sr} , k_{ca} , k'_{sr} and k'_{ca} are dissociation rate constants (cf. Table 1). The parameter η , defined in Eq (2), measures the preference of Cand1 and SR for binding to Cul1. Similarly, α and β account for relative differences in the dissociation rate constants for the binary complexes (α) and the ternary complex (β).

<https://doi.org/10.1371/journal.pcbi.1005869.g001>

model predicts that there exists an optimal Cand1 concentration at which the time scale for substrate degradation becomes minimal. We confirmed this prediction by measuring the half-life of a SCF substrate in cells overexpressing either wildtype Cand1 or a functionally compromised deletion mutant of Cand1. In a second step, we analyzed the Cand1-mediated exchange

of SRs in the presence of substrates through numerical simulations which suggest a crucial role for Cand1 in remodeling the cellular CRL repertoire in response to changing substrate loads.

Models

Model for the Cand1 exchange cycle. In our model (cf. Fig 1B) we considered two species of substrate receptors (SRs) which competitively bind to the Cul1 scaffold via the adapter protein S-phase kinase-associated protein 1 (Skp1) [29]. Here, we did not explicitly model the assembly of Skp1 and SRs, but considered Skp1/SR dimers as preformed stable entities denoted for convenience by SR1 and SR2. Consistent with experiments we assumed that binding of Cand1 to Cul1 lowers the binding affinity for SRs by 6 orders of magnitude [9], i.e. $K'_{sr}/K_{sr} \sim 10^6$, where K_{sr} and K'_{sr} denote the dissociation constants of SRs from the binary Cul1.SR and the ternary Cul1.Cand1.SR complexes, respectively. Throughout the manuscript punctuation between protein names is used to denote non-covalent protein-protein interactions. Similarly, binding of SRs to Cul1 lowers the affinity for Cand1 by the same amount (i.e. $K'_{ca}/K_{ca} \sim 10^6$) resulting in the thermodynamic cycles depicted in Fig 1B. Since the free energy change for the formation of the ternary Cul1.Cand1.SR complexes must not depend on the order in which they are formed the dissociation constants in each cycle must satisfy the detailed balance relation

$$K_{ca} \cdot K'_{sr} = K'_{ca} \cdot K_{sr} \tag{1}$$

Here, K_{ca} and K'_{ca} denote the dissociation constants of Cand1 from the binary Cul1.Cand1 complex and the ternary Cul1.Cand1.SR complexes, respectively. To satisfy the detailed balance condition (1) we introduced the relative binding affinity

$$\eta = \frac{K'_{ca}}{K_{ca}} = \frac{K_{sr}}{K'_{sr}} \tag{2}$$

which measures the preference of Cand1 and SR for binding to Cul1, i.e. $\eta < 1$ means that Cand1 has a higher binding affinity for Cul1 whereas $\eta > 1$ means that SR has a higher binding affinity for Cul1.

To translate the reaction steps depicted in Fig 1B into a mathematical model we employed mass-action kinetics and assumed that the total protein concentrations (Cul1, Cand1, SR1 and SR2) remain constant on the time scale of interest. The dynamics of the system is described by 5 ordinary differential equations

$$\begin{aligned} \frac{dy_1}{dt} &= k_{sr} \left(\frac{[Cul1][SR1]}{K_{sr}} - y_1 \right) - \beta k'_{sr} \left(\frac{y_1 [Cand1]}{\eta K'_{sr}} - y_4 \right) \\ \frac{dy_2}{dt} &= k_{sr} \left(\frac{[Cul1][SR2]}{K_{sr}} - y_2 \right) - \beta k'_{sr} \left(\frac{y_2 [Cand1]}{\eta K'_{sr}} - y_5 \right) \\ \frac{dy_3}{dt} &= \alpha k_{sr} \left(\frac{[Cul1][Cand1]}{\eta K_{sr}} - y_3 \right) - k'_{sr} \left(\frac{y_3 ([SR1] + [SR2])}{K'_{sr}} - (y_4 + y_5) \right) \\ \frac{dy_4}{dt} &= \beta k'_{sr} \left(\frac{y_1 [Cand1]}{\eta K'_{sr}} - y_4 \right) + k'_{sr} \left(\frac{y_3 [SR1]}{K'_{sr}} - y_4 \right) \\ \frac{dy_5}{dt} &= \beta k'_{sr} \left(\frac{y_2 [Cand1]}{\eta K'_{sr}} - y_5 \right) + k'_{sr} \left(\frac{y_3 [SR2]}{K'_{sr}} - y_5 \right) \end{aligned} \tag{3}$$

where y_1, \dots, y_5 denote binary and ternary protein complexes as indicated in Fig 1B. The remaining variables in Eq (3) were expressed in terms of the y_i using the mass conservation

relations

$$\begin{aligned}
 [\text{Cul1}] &= \text{Cul1}_T - (y_1 + y_2 + y_3 + y_4 + y_5) \\
 [\text{SR1}] &= \text{SR1}_T - (y_1 + y_4) \\
 [\text{SR2}] &= \text{SR2}_T - (y_2 + y_5) \\
 [\text{Cand1}] &= \text{Cand1}_T - (y_3 + y_4 + y_5)
 \end{aligned}
 \tag{4}$$

where Cul1_T , SR1_T , SR2_T and Cand1_T denote the total concentrations of Cul1, substrate receptors and Cand1, respectively.

To parametrize our model we employed representative rate constants as they were measured for the SCF^{Fbxw7} ligase (cf. Table 1). The only rate constant that remained undetermined in that study was estimated from transient data in Ref. [10] (see Materials and methods). Since all F-box containing SRs bind Cul1 via the Skp1 adapter protein we assume that both Skp1/SR dimers in Fig 1B exhibit similar binding parameters as Skp1/Fbxw7. This idealized scenario is sufficient for our purpose as it allows studying competition effects between different SRs (through their relative abundances) while keeping the analysis of the system tractable. Later on we relax this assumption and study the impact of different SR binding affinities on the time scale of substrate degradation.

Results

Cand1 reduces SCF ligase activity

We first examined how the presence of Cand1 affects the steady state occupancies of different SCF complexes (i.e. Cul1.SR1 and Cul1.SR2). To this end, we assumed that Cul1 is saturated with SRs, i.e. we considered the physiologically relevant regime $\text{SR}_T = \text{SR1}_T + \text{SR2}_T > \text{Cul1}_T$. From the parameter values listed in Table 1 we see that $\eta K_{sr} \ll \text{Cul1}_T$. Under this condition we derived approximate expressions for the steady state concentration of Cul1.SR1 (and the other complexes) in the limit of low and high concentrations of Cand1 (see Supporting Information S1 Text for details). In the first case ($\text{Cand1}_T \ll \text{Cul1}_T$) the concentration of Cul1.SR1 decreases linearly with Cand1_T according to

$$[\text{Cul1.SR1}] \approx \frac{\text{SR1}_T}{\text{SR}_T} (\text{Cul1}_T - f \cdot \text{Cand1}_T)
 \tag{5}$$

Table 1. Default parameter values.

protein concentrations [nM]	dissociation constants [nM]	dissociation rate constants [s^{-1}]	scale factors (dimensionless)
$\text{Cul1}_T = 300$ ^(a)	$K_{sr} = 2.25 \cdot 10^{-4}$ ^(c)	$k_{sr} = 9 \cdot 10^{-7}$ ^(c)	$\eta = K_{ca}/K_{sr} = 0.077$
SR_T ^(b) = 660 ^(a)	$K'_{sr} = 650$ ^(c)	$k'_{sr} = 1.3$ ^(c)	$\alpha = k_{ca}/k_{sr} = 11.11$
$\text{Cand1}_T = 390$ ^(a)	$K_{ca} = 1.73 \cdot 10^{-5}$ ^(d)	$k'_{ca} = 1 \cdot 10^{-5}$ ^(c)	$\beta = k'_{ca}/k'_{sr} = 0.031$
	$K'_{ca} = 50$ ^(c)	$k'_{ca} = 0.04$ ^(e)	

^(a) Ref. [9],

^(b) $\text{SR}_T = \text{SR1}_T + \text{SR2}_T$,

^(c) Ref. [10],

^(d) computed from Eq (1),

^(e) cf. Materials and Methods.

<https://doi.org/10.1371/journal.pcbi.1005869.t001>

where the slope f is given by

$$f = \frac{K'_{sr} + SR_T - Cul1_T}{K'_{sr} + \left(1 + \frac{\eta K'_{sr}}{Cul1_T}\right) (SR_T - Cul1_T)} \quad (6)$$

In contrast, for large Cand1 concentrations ($Cand1_T \gg Cul1_T$) the concentration of Cul1.SR1 decreases as a power law ($\sim 1/Cand1_T$) according to

$$[Cul1.SR1] \approx \eta K'_{sr} \frac{Cul1_T}{Cand1_T} \frac{SR1_T}{K'_{sr} + SR_T + Cul1_T} \quad (7)$$

By symmetry, there exist similar expressions for [Cul1.SR2] with $SR1_T$ being replaced by $SR2_T$. Note that the slope parameter defined in Eq (6) is limited to the range $0 < f < 1$ where the lower bound is approached if $\eta K'_{sr} \gg Cul1_T$ and vice versa for the upper bound. For the parameters listed in Table 1 we obtain $f \approx 0.94$ which is close to the upper bound. From Eqs (5) and (7) we see that the SCF concentration decreases as a function of $Cand1_T$ which is consistent with previous observations according to which Cand1 acts as an inhibitor of SCF ligase activity [20, 26, 27].

To analyze the behavior of the SCF occupancy near the transition point (where $Cand1_T = Cul1_T$) we plotted the steady state concentration of Cul1.SR1 for different values of the relative binding affinity η (Fig 2A). We find that when $\eta = 1$ or larger the SCF concentration changes gradually near the transition point. However, when Cand1 exhibits a strong preference for binding to Cul1 ($\eta \ll 1$) the SCF response curve develops a sharp threshold near the transition point (black line, Fig 2A). Since the natural system seems to operate in the regime $\eta \ll 1$ and $Cand1_T > Cul1_T$ (cf. Table 1) one might expect that the concentration of SCF complexes (Cul1.SR1 and Cul1.SR2) is low under steady state conditions. However, this line of reasoning could be affected by two factors: First, the effective Cand1 concentration (available for binding to Cul1) could be lower than that of Cul1 because Cand1 also binds to other cullins *in vivo* [9]. Second, in the presence of substrates the concentration of particular SCF complexes could be increased due to dynamic remodeling of the SCF repertoire [8, 10, 24].

Trade-off between high SCF activity and fast SR exchange

Next we analyzed how Cand1 affects the time scale for the exchange of SRs. If Cand1 is a SR exchange factor, as experiments suggest [10, 17, 18], the exchange rate should increase with increasing Cand1 concentration. To quantify the exchange rate we computed the leading eigenvalue of the Jacobian matrix (Fig 2A and S1 Text) which determines the time scale for reaching a new steady state after applying a perturbation. Note that the SR exchange rate (as measured by $|\rho_l|$) dramatically increases when the Cand1 concentration is increased beyond that of Cul1 (the increase being more dramatic as η gets smaller). However, when $Cand1_T$ is increased the SCF concentration ($[Cul1.SR1]$) concomitantly drops resulting in a trade-off between high SCF occupancy at low Cand1 concentration and fast SR exchange at high Cand1 concentration. This trade-off is visualized in Fig 2B where we plotted the SCF exchange rate against SCF occupancy. The resulting curve appears to be independent of the value of η . However, depending on the value of η the cellular Cand1 concentration of 390nM is reached at different positions along the trade-off curve (indicated by symbols). For example, when $\eta = 0.077$ (corresponding to the value in Table 1) the SCF concentration is 6.4nM and the exchange rate is $0.11s^{-1}$.

To illustrate the impact of Cand1 on the time scale of SR exchange we assumed that at $t = 0$ a fixed amount of SR1 is added to a steady state mixture of Cul1, Cand1 and SR2 with

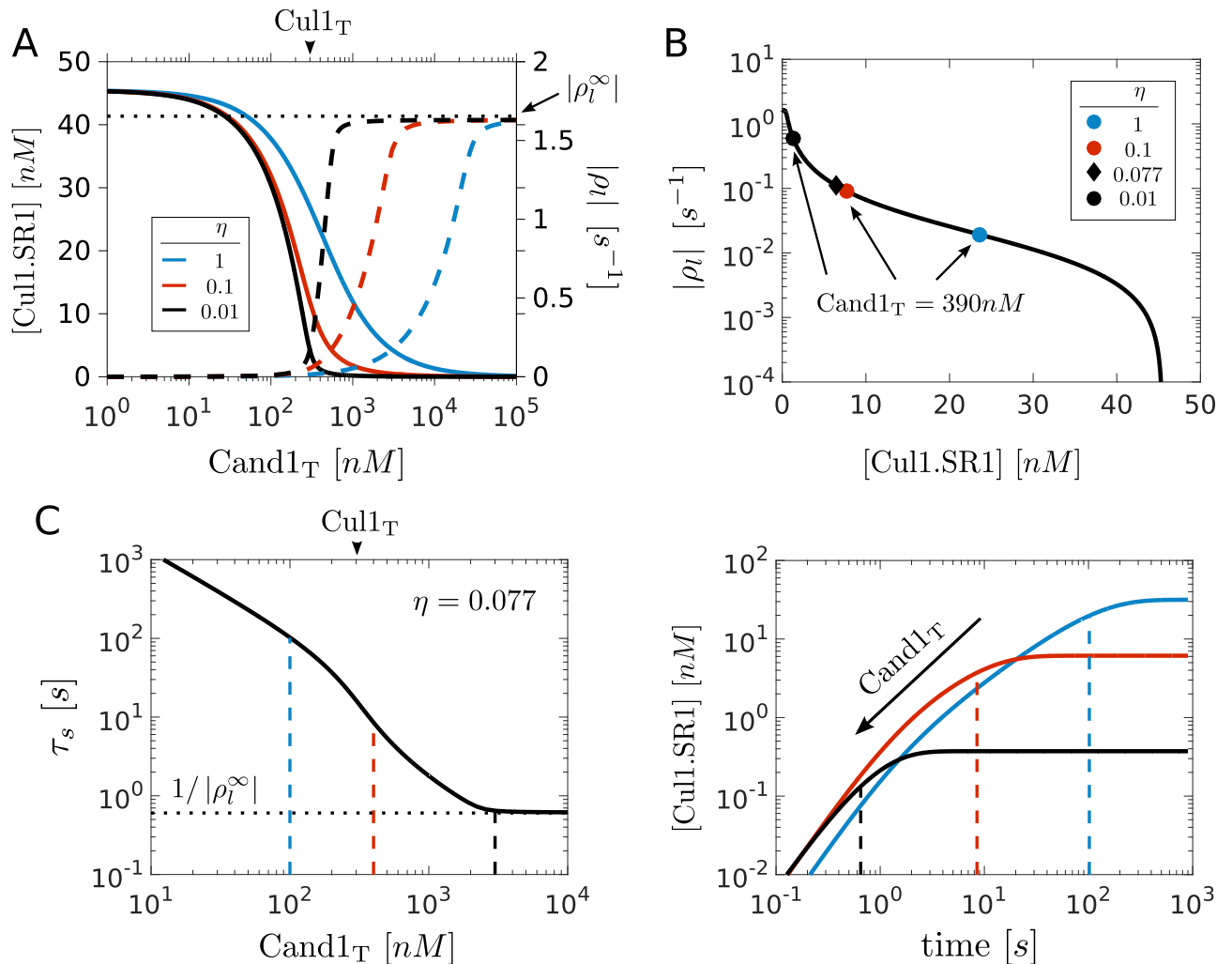


Fig 2. Trade-off between high SCF occupancy and fast SR exchange rate. **A:** Left axis shows SCF activity as measured by the steady state concentration of Cul1.SR1. Right axis shows the exchange rate as measured by the leading eigenvalue of the Jacobian matrix (ρ). As the total Cand1 concentration increases the SCF activity (solid lines) decreases while the exchange rate (dashed lines) concomitantly increases. As the relative binding affinity η (Eq 2) decreases both the SCF response curve as well as the curve characterizing the exchange rate develop a sharp threshold near $Cand1_T = Cul1_T$ (marked by arrow head). The horizontal dotted line indicates the maximal exchange rate (cf. Eq 9). **B:** Exchange rate ($|\rho|$) vs. SCF occupancy ([Cul1.SR1]) drawn from the curves in panel A. Note that the curves are overlapping. We have also indicated the positions along the curve where, depending on the value of η , the concentration of Cand1 equals that observed in cells (cf. Table 1). **C:** Left panel shows the time scale for the exchange of substrate receptors ($\tau_s = 1/|\rho|$) as a function of the total Cand1 concentration for the parameters listed in Table 1. Right panel shows the corresponding time course for the assembly of Cul1.SR1 after adding 100nM SR1 to a steady-state mixture containing 300nM Cul1, 560nM SR2 and Cand1 as indicated by the dashed lines in the left panel. The dashed lines in the right panel indicate the value of τ_s obtained from the intersection of the dashed lines with the black solid line in the left panel.

<https://doi.org/10.1371/journal.pcbi.1005869.g002>

SR2_T > Cul1_T so that the cullin scaffold is already saturated with SRs prior to addition of SR1. After SR1 is added, a certain fraction of it gets exchanged for SR2 on Cul1. The time scale for the assembly of Cul1.SR1 ranges from a few minutes when Cand1_T ≪ Cul1_T to a few seconds when Cand1_T ≫ Cul1_T (cf. Fig 2C).

To understand the constraints under which Cand1 mediates the exchange of SRs we considered again the two limiting regimes: Cand1_T ≪ Cul1_T and Cand1_T ≫ Cul1_T. In the first

case the leading eigenvalue can be approximated by (cf. S1 Text)

$$|\rho_l| \approx k_{sr} + \frac{1}{\frac{1}{k'_{sr}} + \frac{1}{\beta k'_{sr}}} \frac{\text{Cand1}_T}{K'_{sr}}. \quad (8)$$

Consistent with expectation: As $\text{Cand1}_T \rightarrow 0$, the SR exchange rate approaches the (spontaneous) dissociation rate constant of a Cul1.SR complex which is in the order of 10^{-6} s^{-1} (cf. Table 1). In the presence of Cand1 the first term in Eq (8) can be neglected showing that at low Cand1 concentrations the SR exchange rate is determined by the total rate with which the ternary complex dissociates into either of the two binary complexes, i.e. both branches (Cul1.Cand.SR \rightarrow Cul1.SR and Cul1.Cand.SR \rightarrow Cul1.Cand) contribute to the total dissociation rate. In contrast, if $\text{Cand1}_T \gg \text{Cul1}_T$ the SR exchange rate approaches a limiting value that is independent of η and Cand1_T (cf. Fig 2A)

$$|\rho_l^\infty| \approx k'_{sr} \left(1 + \frac{\text{Cul1}_T}{K'_{sr}} \frac{\text{Cul1}_T + K'_{sr}}{\text{Cul1}_T + \text{SR}_T + K'_{sr}} \right). \quad (9)$$

Since this expression depends on k'_{sr} and K'_{sr} (but not on k'_{ca} and K'_{ca}) it is the dissociation rate of the ternary complex towards Cul1.Cand1 which ultimately limits the rate with which new SRs can gain access to Cul1.

Optimal Cand1 concentration

Due to the opposing effects of Cand1 on the SCF levels and the SR exchange rate we next asked how Cand1 affects the substrate degradation rate. To this end, we extended the model depicted in Fig 1B by assuming that substrate reversibly binds to Cul1.SR1 and that the substrate in the Cul1.SR1.S1 complex can be degraded by the proteasome (Fig 3A). Here, we did not attempt to model the substrate degradation process in detail, instead we lumped the relevant steps of the CRL cycle depicted in Fig 1A (neddylation, ubiquitylation, deneddylation) into a single first order rate constant (k_{deg}). To mimic the effect of neddylation we assumed that once substrate is bound to its cognate SR the corresponding ligase complex becomes inaccessible for Cand1 so that SR exchange is suppressed [14, 25]. This assumption is consistent with the fact that substrate binding triggers neddylation and inhibits deneddylation, events that render the cullin unable to bind Cand1 [30, 31]. To study the effects of Cand1 on the substrate degradation rate we performed numerical simulations where the total amount of SRs was partitioned into 30nM SR1 and 630nM SR2. Then, a ten-fold excess of substrate for SR1 ($\text{SR1}_T = 300\text{nM}$) was added to a steady state mixture of Cul1, SR1, SR2 and different amounts of Cand1. Interestingly, the time scale for substrate degradation (measured by the time $t_{1/2}$ it takes to degrade half of the total substrate) exhibited a non-monotonous behavior as a function of Cand1_T (Fig 3B) changing from 48min ($\text{Cand1}_T = 0\text{nM}$) to 28min ($\text{Cand1}_T = 100\text{nM}$) and then to 95min ($\text{Cand1}_T = 1000\text{nM}$). Hence, there exists a minimum of $t_{1/2}$ at intermediate Cand1 concentrations (Fig 3C).

The exchange of SRs by Cand1 takes time. So, we reasoned that Cand1 would lose its ability to accelerate substrate degradation if the binding affinity of the substrate for its cognate SR became too low. This is, indeed, what we observed (Fig 3C): As the binding affinity decreases (k_{on} decreases) the minimum vanishes and $t_{1/2}$ increases monotonously with Cand1_T suggesting that Cand1 loses its ability to speed up substrate degradation for low-affinity substrates. Moreover, if Cand1_T becomes larger than $\text{Cul1}_T = 300\text{nM}$ the $t_{1/2}$ substantially rises independently of k_{on} indicating that this regime might be unfavorable for efficient substrate degradation.

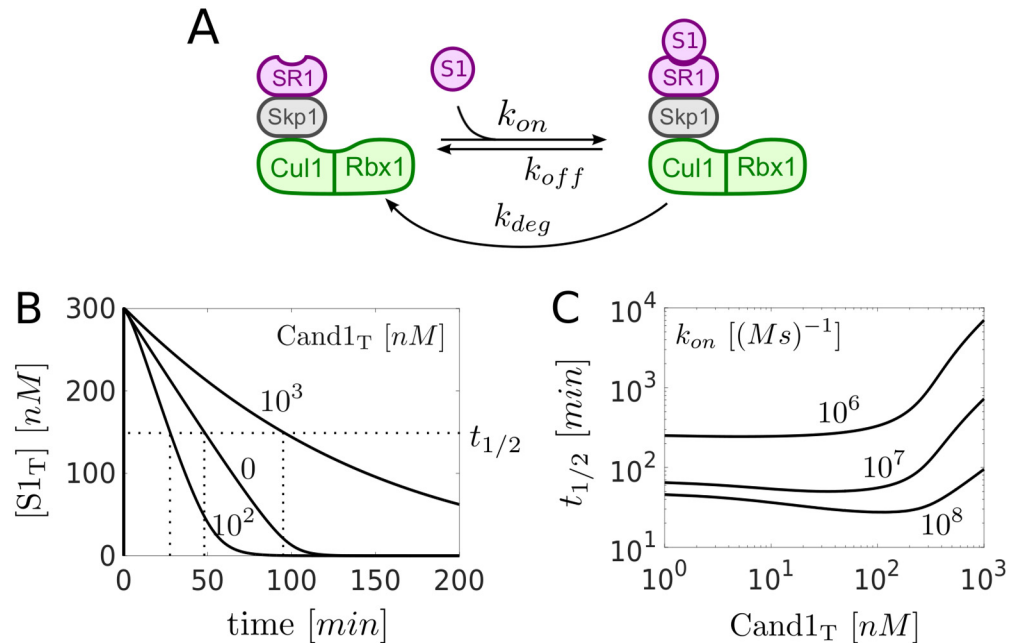


Fig 3. Optimal Cand1 concentration. **A:** Extension of the model depicted in Fig 1B. Substrate (S1) reversibly binds to Cul1.SR1. The substrate in the resulting Cul1.SR1.S1 complex is degraded with effective rate constant k_{deg} . **B:** Time courses showing the degradation of total substrate $S_T = [S1] + [Cul1.SR1.S1]$. At $t = 0$ substrate (300nM) was added to a steady state mixture containing $SR1_T = 30nM$, $SR2_T = 630nM$ and $Cand1_T$ as indicated. Note that $t_{1/2}$ changes non-monotonically as a function of $Cand1_T$. **C:** Half-life for substrate degradation ($t_{1/2}$) as a function of $Cand1_T$ for decreasing binding affinity. As the association rate constant k_{on} for substrate binding decreases $t_{1/2}$ increases and the dependence of $t_{1/2}$ on $Cand1_T$ becomes monotonic. Parameters for substrate binding: $k_{on} = 10^8 M^{-1} s^{-1}$, $k_{off} = 1 s^{-1}$, $k_{deg} = 0.004 s^{-1}$. Parameters other than those mentioned are listed in Table 1.

<https://doi.org/10.1371/journal.pcbi.1005869.g003>

Altering endogenous Cand1 levels delays SCF-mediated substrate degradation

To experimentally test the concept of an optimal Cand1 concentration *in vivo*, we manipulated Cand1 levels in *S. pombe* cells, and determined the effect on the degradation the CDK inhibitor Rum1p. The latter represents a well-established substrate of an SCF^{Pop1p/Pop2p} complex [32–35] that was previously shown to be regulated by Cand1 [17]. We created strains conditionally overexpressing wildtype Cand1 or a deletion mutant of Cand1 missing the C-terminal β -hairpin loop (residues 1063-1074, Cand1 Δ - β HP). When Cand1 is bound to Cul1, its β -hairpin loop prevents the recruitment of SR to Cul1 due to steric clash with Skp1 [27]. Cand1 Δ - β HP, in turn, can form stable Cand1.Cul1.SR ternary complexes *in vitro* [27] and is thus predicted to be deficient in exchange factor activity. Since catalytically inactive Cand1 Δ - β HP can still bind Cul1 [27], it is expected to compete with endogenous Cand1 in a dominant negative fashion thus essentially mimicking a Cand1 deletion. The Cand1 overexpression strains also had their endogenous genomic *rum1* ORF modified with Myc epitope tags for facile detection by immunoblotting with Myc antibodies.

Upon promoter induction, the effect of Cand1 overexpression on Rum1p stability was assessed in cycloheximide chase experiments. Whereas Rum1p had a half-life of 10.1 (+/- 1.85) minutes in the empty vector control strain, its half-life was increased to 15.88 (+/- 1.44, $p = 0.07$) minutes in cells overexpressing wildtype Cand1 (Fig 4). Likewise, overexpression of Cand1 Δ - β HP increased Rum1p half-life to 20.86 (+/- 5.78, $p = 0.11$) minutes, suggesting

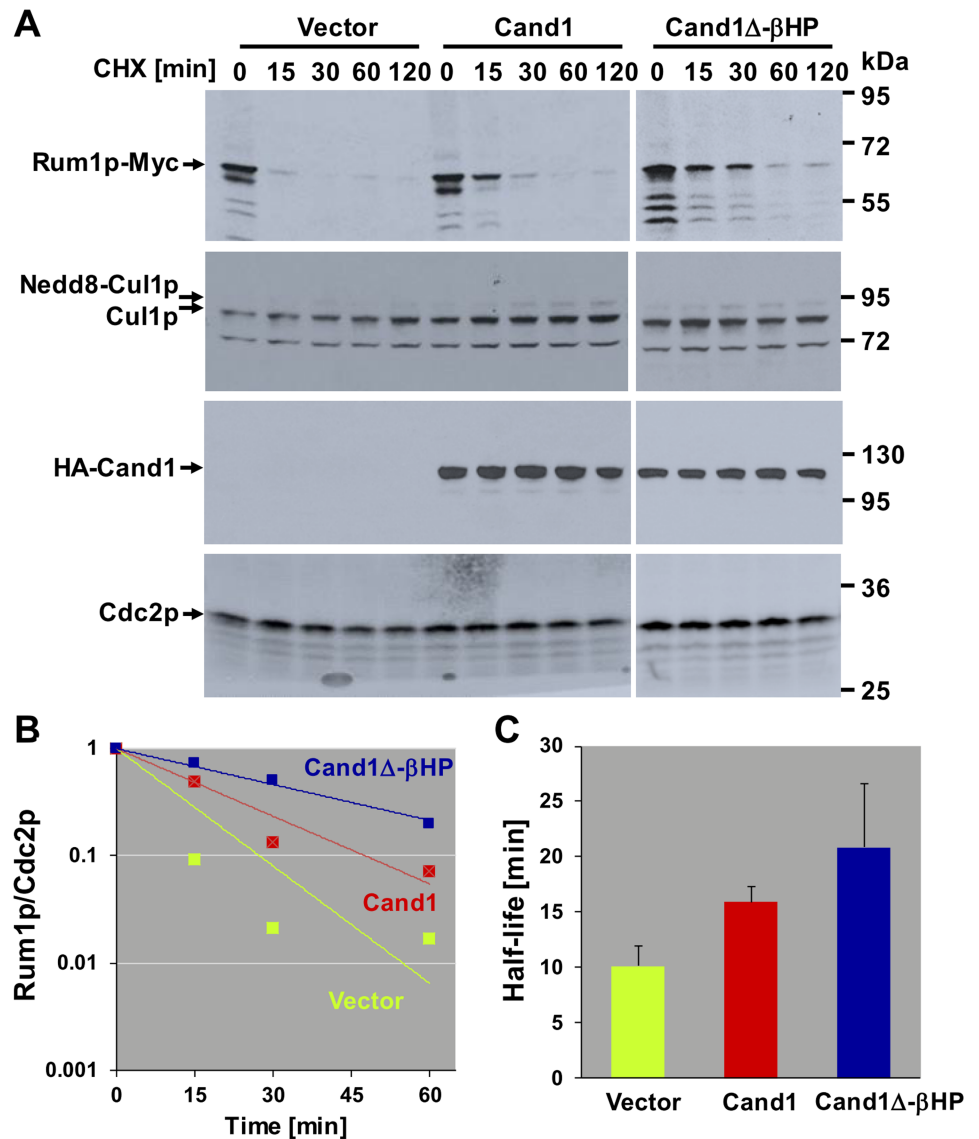


Fig 4. Effect of Cand1 dose on the stability of the SCF substrate Rum1p in *S. pombe*. **A:** *S. pombe* cells stably overexpressing the indicated versions of Cand1 were treated with 100 $\mu\text{g/ml}$ cycloheximide (CHX) for the indicated periods of time and analyzed for the expression of Rum1p, Cul1p, and Cand1 by immunoblotting. Cdc2p signals are shown for reference. Representative results of two independent experiments. **B:** Immunoblotting signals for Rum1p and Cdc2p were quantified using Image Studio Lite, and Rum1p intensities normalized to Cdc2p were plotted on a log scale. **C:** Exponential decay lines fitted through the data points in (B) were used to calculate protein half-lives in strains overexpressing the indicated Cand1 proteins. Results are averages of two independent experiments. Error bars represent standard deviations.

<https://doi.org/10.1371/journal.pcbi.1005869.g004>

dominant negative interference with Rum1p proteolysis. Neither Cand1 species had any effect on steady-state Cul1 neddylation (Fig 4A), suggesting that the effect on Rum1p stability is not mediated through altering ligase activation by Nedd8. Thus, both an excess of dominant positive or dominant negative Cand1 delays SCF-dependent substrate degradation (Fig 4B and 4C). Together, these findings confirm our model prediction and suggest that Cand1 concentration in cells is tuned within a narrow margin such as to maximize the substrate degradation rate.

Dynamic readjustment of the SCF repertoire

To increase the pool size of SCF ligases that can be directed against a cognate substrate unused SCF complexes should first be disassembled making the freed Cul1 available for re-assembly into a new SCF. This process is simulated in Fig 5: After addition of substrate the initial drop in [Cul1.SR2] is compensated by an increase in [Cul1.SR1.S1] (Fig 5A). Later on, between 1-100min, the concentration of Cul1.SR1.S1 further rises due to disassembly of Cul1.SR2 and redistribution into Cul1.SR1 and Cul1.SR1.S1. The sum of the concentrations of these “engaged” SCF ligases ([Cul1.SR1]+[Cul1.SR1.S1]) increases 2.5-fold from its steady state value before it decreases back to pre-stimulus level after the substrate has been degraded (Fig 5B, solid violet line). The remaining curves indicate the contribution from each of the other

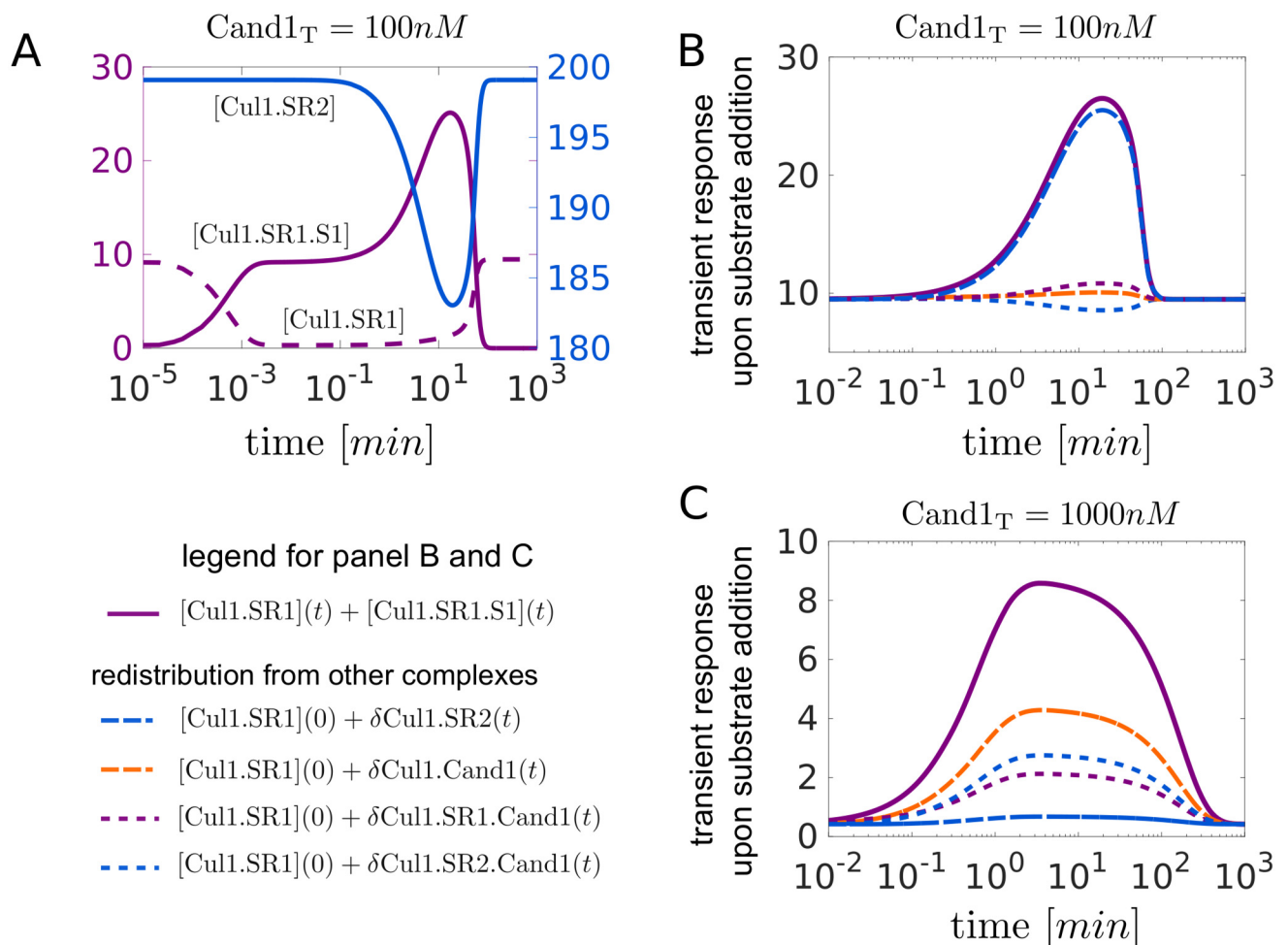


Fig 5. Dynamic readjustment of the SCF repertoire. **A:** Transient response of the SCF complexes Cul1.SR1, Cul2.SR2 and Cul1.SR1.S1 upon substrate addition (300nM at $t = 0$) to a steady state mixture containing $SR1_T = 30nM$, $SR2_T = 630nM$ and $Cand1_T = 100nM$. Between 1-100min the drop in [Cul1.SR2] is accompanied by a peak in [Cul1.SR1.S1] indicating that Cul1 is redistributed from Cul1.SR2 into Cul1.SR1 and Cul1.SR1.S1. **B, C:** Redistribution of Cul1 from Cul1.SR2, Cul1.SR1(2).Cand1 and Cul1.Cand1 into Cul1.SR1 and Cul1.SR1.S1 for $Cand1_T = 100nM$ (B) and $Cand1_T = 1000nM$ (C). In both panels the solid violet line shows the transient increase of the concentration of “engaged” ligases ([Cul1.SR1] + [Cul1.SR1.S1]) upon substrate addition as described in (A). The remaining curves indicate the contribution to the transient response by any of the other complexes. For example, $\delta Cul1.SR2(t) = [Cul1.SR2](t) - [Cul1.SR2](0)$ denotes the amount of Cul1 that is redistributed into Cul1.SR1 and Cul1.SR1.S1 upon disassembly of Cul1.SR2. Note that in panels B and C the solid violet curve is the sum of the other curves. Parameters for substrate binding: $k_{on} = 10^8 M^{-1} s^{-1}$, $k_{off} = 1 s^{-1}$, $k_{deg} = 0.004 s^{-1}$. Parameters other than those mentioned are listed in Table 1.

<https://doi.org/10.1371/journal.pcbi.1005869.g005>

complexes (resulting from disassembly of Cul1.SR2, Cul1.SR1.Cand1, Cul1.SR2.Cand1 and Cul1.Cand1) assuming that redistribution of Cul1 occurred from only one of these complexes. Hence, at low Cand1 concentrations the majority of the redistributed Cul1 comes from Cul1.SR2 (Fig 5B, blue line, long dashes) whereas at high Cand1 concentrations (Fig 5C) the main contribution comes from Cul1.Cand1 (orange line, long dashes) and the ternary complexes (short dashes).

Temporal hierarchy of substrate degradation

To address the question whether the Cand1-mediated exchange can induce a temporal order in which SR substrates are targeted for degradation we extended the model depicted in Fig 1B and considered 3 types of SRs: two for which substrates are available (SR1 and SR2) and one representing the remaining SR pool (SR3). It is assumed that downstream processing by the proteasome is the same for both substrates ($k_{deg} = 0.004s^{-1}$), but that there might be differences in the binding affinity of substrate to their cognate SR (Fig 6A and 6D), differences in the binding affinity of SRs to Cul1 (Fig 6B and 6E) or differences in SR abundances (Fig 6C and 6F). Our simulations suggest that differences in either of these parameters can induce a temporal order in the degradation of substrates such that high-affinity substrates, substrates with high-affinity SRs and substrates of highly abundant SRs are degraded first (as indicated by a lower

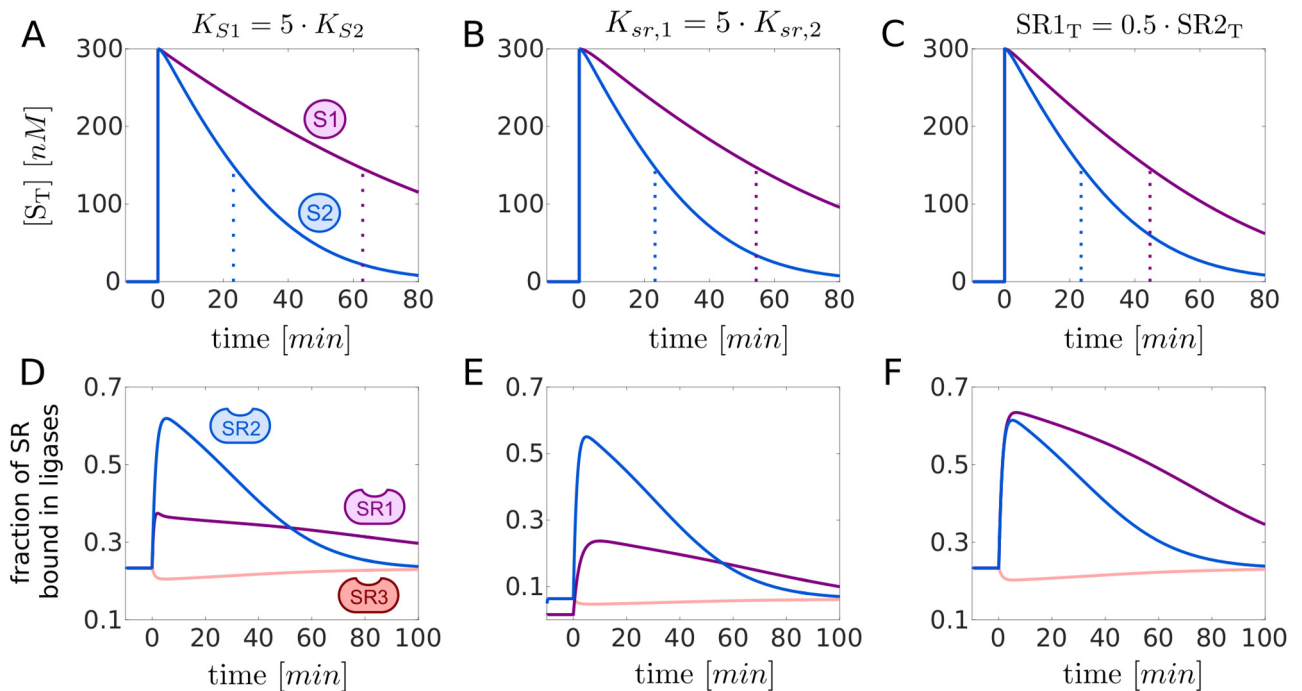


Fig 6. Temporal hierarchy of substrate degradation. **A, B, C:** Transient response upon substrate addition. At $t=0$ two substrates, S1 and S2 (each 300nM), are added to a steady state mixture containing Cul1, Cand1 and SR1-SR3. The resulting decline of the total amount of substrates is displayed together with the $t_{1/2}$ (dotted lines). Substrates with a higher SR affinity (A), substrates for SRs with a higher affinity for Cul1 (B) and substrates for more abundant SRs (C) are preferentially degraded. **D, E, F:** Assembly and disassembly of SCF ligases upon substrate addition. Depicted are changes in the fraction of SRs that are bound in a SCF complex. The blue and violet curves correspond to $([Cul1.SR1] + [Cul1.SR1.S1])/SR1_T$ and $([Cul1.SR2] + [Cul1.SR2.S2])/SR2_T$, respectively, whereas the light red curve denotes $[Cul1.SR3]/SR3_T$. In each case Cul1 is redistributed from Cul1.SR3 into Cul1.SR1(S1) and Cul1.SR2(S2). In (A-F) if not indicated otherwise reference parameters are: $K_{S1} = K_{S2} = 10nM$ ($k_{off} = 1s^{-1}$), $K_{sr,1} = K_{sr,2} = K_{sr,3} = 0.225pM$, $SR1_T = SR2_T = 60nM$. To preserve detailed balance $K'_{sr,1}$ has been increased by a factor of 5 in (B) and (E). $SR3_T = 660nM - (SR1_T + SR2_T)$, $Cand1_T = 400nM$, $k_{deg} = 0.004s^{-1}$. Parameters other than those mentioned are listed in Table 1.

<https://doi.org/10.1371/journal.pcbi.1005869.g006>

$t_{1/2}$). In all cases substrate degradation is accompanied by a redistribution of Cul1 from the pool of unused SCFs (SCF3) into the pool of engaged SCFs (SCF1 and SCF2) supporting the view that in the presence of substrates the exchange activity of Cand1 leads to the preferential assembly of SCFs for which substrates are available [10, 24].

Is Cand1 necessary for fast SR exchange?

One of the puzzling properties of SCF ligases (and perhaps other CRLs) is the extremely high, picomolar affinity of the Cul1-SR interaction [10]. One might speculate that this high affinity prevents “leakage” of SRs from Cul1 so that SR exchange is exclusively mediated by Cand1. In support of this idea, experiments in Cand1 knockdown/knockout cells have shown that many F-box proteins rely on the exchange activity of Cand1 for efficient substrate degradation [17, 18, 23]. Alternatively, one could envision a hypothetical system with substantially weaker Cul1-SR interaction. In such a system newly synthesized F-box proteins could always gain access to Cul1 making an exchange factor dispensable.

To compare these two architectures we rescaled the dissociation rate constant k_{sr} by a factor $\gamma \gg 1$ which lowers the binding affinity between Cul1 and SR (Fig 7A). To satisfy the detailed balance condition in Eq (1) we multiplied k_{ca} by the same factor so that the dissociation constants K_{sr} and K_{ca} increase with γ while their ratio remains constant. In this setting the case $\gamma = 1$ and $\text{Cand1}_T = 390nM$ corresponds to the natural system whereas the case $\gamma \gg 1$ and $\text{Cand1}_T = 0nM$ represents the alternative system design. To make a fair comparison we chose γ such that the steady state level of Cul1.SR1 prior to addition of substrate (S1) is the same for both cases. In addition, we assumed that substrate can bind to both Cul1.SR1 and Cul1.Cand1.SR1. To mimic the effect of neddylation in this setting we allowed substrate to be degraded only when it is bound to Cul1.SR1, but not when it is bound to Cul1.Cand1.SR1 (since Cand1 and Nedd8 cannot be simultaneously bound to Cul1) [27].

Interestingly, the half-life of substrate degradation depends not only on the presence or absence of Cand1, but also on the detailed mechanism of substrate binding (Fig 7A): If substrate can only bind to SR when the latter is already bound to Cul1 or Cul1.Cand1 (sequential mechanism, blue lines) the system without Cand1 (-Cand1) exhibits faster substrate degradation (3.4-fold) compared to the system with Cand1 (Fig 7B, upper panel). In contrast, if substrate can also bind to free SRs and SR.S can bind to Cul1 and Cul1.Cand1 (random order mechanism, red lines) the situation is reversed as substrate degradation is now faster (4.1-fold) in the presence of Cand1 (Fig 7C, upper panel).

There are two factors that might explain this behavior: First, for the system without Cand1 redistribution of Cul1 from Cul1.SR2 into Cul1.SR1 and Cul1.SR1.S1 appears to take place only if substrate binding occurs sequentially (Fig 7B and 7C lower panels). Second, when binding occurs randomly substrate may become “trapped” in SR1.S1 complexes in a system without Cand1. Since in such a system the Cul1-SR binding affinity ($\gamma K_{sr} \approx 37nM$) is weaker than the assumed substrate affinity ($1nM$) binding to free SRs effectively reduces the substrate’s affinity for gaining access to Cul1 which causes the delay in its degradation. Together, these findings suggest that F-box proteins which rely on Cand1 for efficient substrate degradation bind to substrates and Cul1 in a random order.

Discussion

Cullin-RING ubiquitin ligases (CRLs) are multisubunit protein complexes where exchangeable substrate receptors (SRs) assemble on a cullin scaffold to mediate ubiquitylation and subsequent degradation of a large variety of substrates. Motivated by the observation that the exchange of different SRs is catalyzed by an exchange factor (Cand1) [10, 17, 18] we were

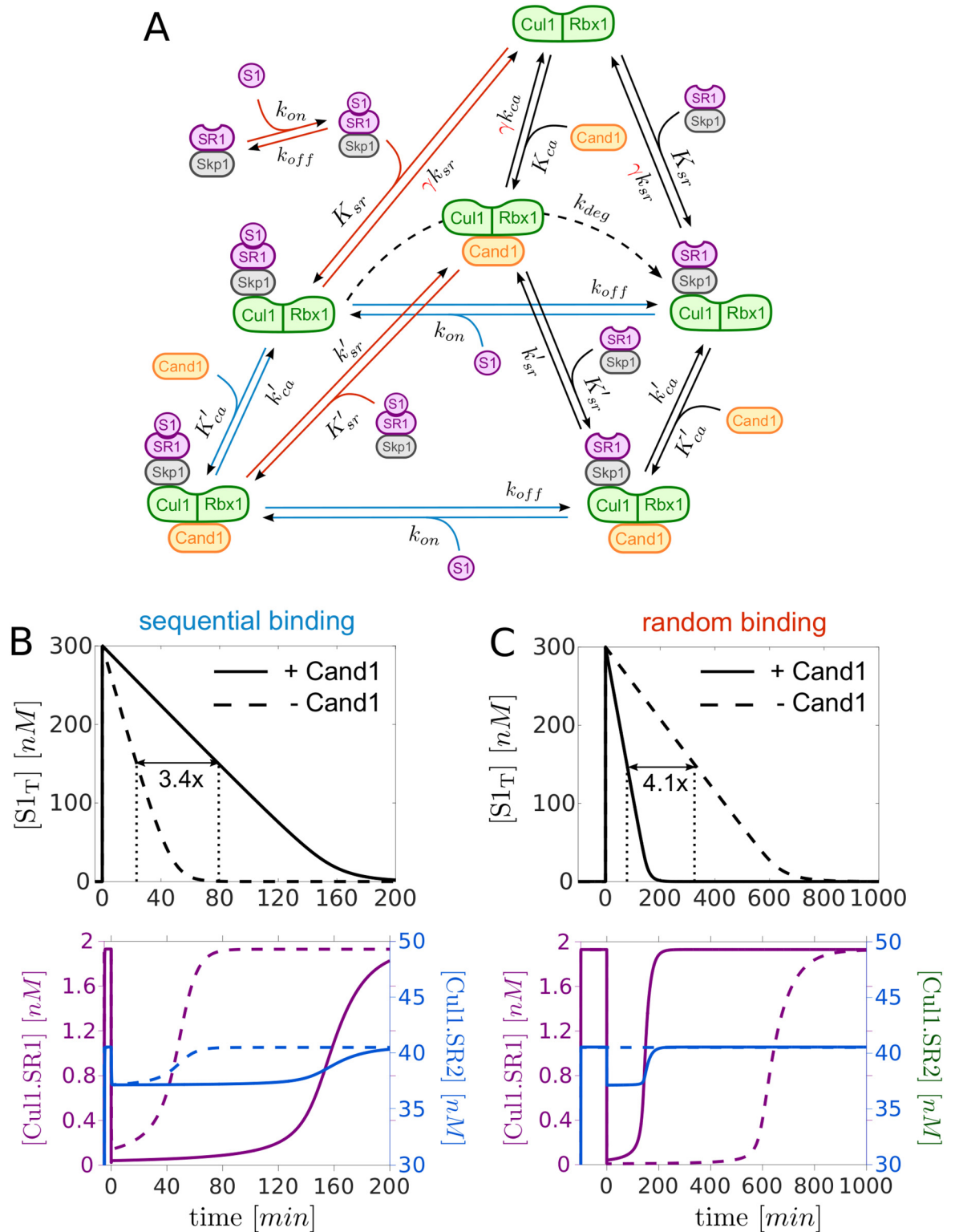


Fig 7. Alternative network architecture. **A:** Extension of the Cand1 cycle model (black solid lines) to analyze different modes of substrate binding to SR1. Sequential mechanism: Substrate (S1) only binds to SR1 if the latter is already bound to Cul1 or Cul1.Cand1 (blue lines). Random order mechanism: S1 binds to free SR1, Cul1.SR1 and Cul1.Cand1.SR1. In addition, SR1.S1 binds to Cul1 or Cul1.Cand1 (red lines). By increasing the factor γ the binding affinity between Cul1 and SR1 can be lowered while still satisfying the detailed balance condition in Eq 1. For SR2 we used the scheme depicted in Fig 1B (without substrate),

but with k_{sr} and k_{ca} multiplied by γ . K_{sr} , K_{ca} , K'_{sr} and K'_{ca} denote dissociation constants whereas k_{sr} , k_{ca} , k'_{sr} and k'_{ca} are dissociation rate constants (cf. Table 1). **B** and **C**: Comparison of the half-life ($t_{1/2}$) of S1 for two network designs: one with Cand1 (+Cand1) and tight binding of SRs to Cul1 (Cand1_T = 390nM, $\gamma = 1$) and another one without Cand1 (-Cand1) and weak binding of SRs to Cul1 (Cand1_T = 390nM, $\gamma = 1.67 \cdot 10^7$). In the latter case γ is chosen such that the pre-stimulus steady state for Cul1.SR1 is the same in both cases (note that dashed and solid lines in lower panels partially overlap). If substrate binds sequentially the system without Cand1 (B, dashed line) outperforms the system with Cand1 (B, solid line) as the $t_{1/2}$ is 3.4-fold larger in the presence of Cand1. In both cases Cul1 is redistributed from Cul1.SR2 to Cul1.SR1 and Cul1.SR1.S1 (B, lower panel). In contrast, when substrate binds in a random order (cf. panel A) its degradation is substantially delayed (4.1-fold) in the absence of Cand1 (C, dashed line) and redistribution of Cul1 only occurs in the presence of Cand1 (C, lower panel). Total substrate is defined as $S1_T = [S1] + [SR1.S1] + [Cul1.SR1.S1] + [Cul1.Cand1.SR1.S1]$. Parameters: At $t = 0$ substrate S1 (300nM) was added to a steady state mixture containing Cul1_T = 300nM, SR1_T = 30nM and SR2_T = 630nM. The values of Cand1_T and γ are indicated in the upper panels. $k_{on} = 10^7 M^{-1} s^{-1}$, $k_{off} = 0.01 s^{-1}$, $k_{deg} = 0.004 s^{-1}$. Parameters other than those mentioned are listed in Table 1.

<https://doi.org/10.1371/journal.pcbi.1005869.g007>

interested in the operating regimes and the inherent constraints that may exist in such exchange systems, and how they would affect the degradation of ubiquitylation substrates. Specifically, we wanted to understand how the CRL network can flexibly react to changing substrate loads despite the high-affinity of cullin-SR interactions.

Trade-off and optimal Cand1 concentration

Our results indicate that there exists a generic trade-off in the Cand1-mediated exchange of SRs which leads to an optimal Cand1 concentration where the time scale for substrate degradation becomes minimal (cf. Fig 3C). This result can be rationalized as follows: In the absence of Cand1 only preassembled SCF complexes contribute to substrate degradation since free SRs cannot gain access to Cul1. As the Cand1 concentration increases the concentration of preassembled SCF complexes decreases since part of the Cul1 is sequestered by Cand1 into Cul1.Cand1 and ternary Cul1.Cand1.SR complexes, which are necessary to mediate the exchange of SRs. However, in the presence of Cand1 disassembly and reassembly of SCFs increases the effective pool size of SCF ligases for a particular substrate at the expense of unused SCF ligases which more than compensates the drop of preassembled SCFs and reduces the time scale for substrate degradation. If, on the other hand, the Cand1 concentration becomes substantially larger than that of Cul1 sequestration of Cul1 into Cul1.Cand1 and ternary complexes dominates. In this regime the drop of preassembled SCFs cannot be compensated anymore by the increased exchange activity of Cand1 resulting in an increased time scale for substrate degradation. Together, these results show that, by lowering the SCF occupancy, the exchange activity of Cand1 necessarily leads to an apparent reduction of SCF ligase activity which is consistent with previous reports of Cand1 acting as an inhibitor of SCF ligases [13, 20, 25–28].

Experimental evidence for optimality

To provide experimental evidence for an optimal Cand1 concentration *in vivo* we have measured the half-life of a SCF substrate in *S. pombe* cells overexpressing dominant positive and dominant negative forms of Cand1 both of which delayed substrate degradation compared to the wildtype (Fig 4). Similar experiments were done by Lo and Hannink in human cell lines [23]. They found that both overexpression of Cand1 as well as siRNA-mediated knockdown of Cand1 leads to increased steady state levels of the transcription factor Nrf2. The latter is an ubiquitylation target of the Cul3-Keap1 ubiquitin ligase whose assembly was shown to be controlled by Cand1 [36] suggesting that our results may not only apply to SCF ligases, but also to other members of the CRL family. Based on the measured rate constants listed in Table 1 our model predicts an optimal Cand1 concentration in the range between 30nM–120nM depending on the substrate's binding affinity. When comparing this prediction with the cellular

concentrations of Cand1 (390nM) and Cul1 (302nM) one has to take into account that Cand1 not only binds to Cul1, but also to cullins of other CRL family members (Cul2-Cul5) whose total concentration adds up to $\approx 1260\text{nM}$ [9]. Hence, the *in vivo* Cand1/CRL ratio of ~ 0.3 falls onto the upper boundary of the predicted range of optimal Cand1 concentrations indicating that in cells the exchange activity of Cand1 might be optimized for high-affinity substrates. In fact, our simulations show that Cand1 loses its ability to speed up substrate degradation when the substrate's binding affinity becomes too low (Fig 3C).

Temporal hierarchy and “on demand” architecture

Through numerical simulations we found that variations in biochemical parameters such as substrate-SR affinities can induce a temporal order for the degradation of substrates such that high-affinity substrates are degraded first (Fig 6). Similar effects are observed for high-affinity and highly abundant SRs suggesting that cells may exploit several mechanisms to fine-tune substrate degradation to needs. Our simulations also showed that in the presence of substrate unused SCF complexes are disassembled making the freed Cul1 available for re-assembly into SCF complexes that are engaged in substrate degradation (Fig 5). This finding supports previous ideas according to which SCF substrates may bias the SCF repertoire leading to the preferential assembly of those SCFs for which substrates are available [10, 24]. Together, our results suggest that Cand1 may endow the CRL network with the flexibility of an “on demand” system, thereby allowing cells to dynamically adjust their CRL repertoire to fluctuating substrate abundances.

Comparison with GDP/GTP exchange systems

From a mechanistic point of view the Cand1-mediated exchange of SRs exhibits some similarity to the exchange of GDP by GTP as mediated by guanosine nucleotide exchange factors (GEFs) [19]. However, while GEFs catalyze the exchange between only two substrates, Cand1 potentially mediates the exchange of hundreds of different SRs. When comparing the parameters of the Cand1 cycle with those of GDP/GTP exchange cycles one finds several systems that seem to operate in a similar regime. For example, in the Ran/RCC1 as well as in the EF-Tu/EF-Ts systems the concentration of the exchange factors, RCC1 and EF-Ts, is typically lower than that of the respective GDP/GTP-binding proteins [37, 38]. Also, the binding affinities of GDP and the exchange factor with respect to EF-Tu or Ran are either comparable [39] or there exists a slight preference in favor of the exchange factor [37] suggesting that both systems operate in the regime $\eta \leq 1$. Similar as for the Cand1 cycle this may indicate that the concentration of the respective exchange factor is optimized for the purpose of the system, e.g. fast nuclear export rate of proteins in the case of Ran/RCC1 and a high protein synthesis rate in the case of EF-Tu/EF-Ts. Indeed, theoretical studies have shown that GDP/GTP exchange systems potentially exhibit similar trade-offs as the ones reported here for the Cand1 cycle [40, 41] although direct experimental evidence for an optimized concentration of the exchange factor seems to be lacking in those cases.

Materials and methods

Experiments

The *S. pombe* *knd1* gene (SPAC1565.07c), encoding the ortholog of human Cand1, was cloned into the pREP3-HA vector, which drives the expression of N-terminal HA-tagged proteins from the thiamine repressible *nmt1* promoter. Two Cand1 mutants were constructed in the same expression vector. The first mutant lacked the N-terminal 32 amino acid and the second

mutant lacks residues 1063-1074, corresponding to the β -hairpin loop. The plasmids were transformed into a strain carrying a Myc-tagged allele of *rum1* at the endogenous genomic locus (*rum1-13myc*) [35]. The expression of Cand1 was induced by removal of thiamine from the culture medium for 20 h, and 100 $\mu\text{g/ml}$ freshly prepared cycloheximide was added. Cells were harvested at the time points indicated in Fig 4A. Cell lysates were prepared by bead lysis in 2x sample buffer and were analyzed by immunoblotting with antibodies directed against MYC (Cell Signaling 2276, 1:1000), HA (Abcam 16918, 1:1000), Cul1p (1:500) [35] and Cdc2 (Santa Cruz, sc-53p (PSTAIRE) 1:500).

Modeling

The simulations depicted in Fig 2 were done using MatCont [42]. The transient simulations involving substrate degradation depicted in Figs 3 and 5–7 were done using the SimBiology Toolbox of MATLAB [43]. Derivations of the analytical formulas in Eqs (5)–(9) can be found in S1 Text.

Model extensions: Substrate binding and 3 substrate receptors. To generate the simulations depicted in Figs 3 and 5 we have assumed that substrate (S1) reversibly binds to its cognate substrate receptor (Skp1/SR1) with forward and backward rate constants k_{on} and k_{off} . Not much seems to be known about the values of these parameters for particular substrates, so we set $k_{on} = 10^8 \text{M}^{-1}\text{s}^{-1}$ (close to the diffusion limit) and $k_{off} = 1 \text{s}^{-1}$ giving a binding affinity of $K_D = k_{off}/k_{on} = 10 \text{nM}$. Given the tight binding between Cul1 and SRs ($K_D \sim 1 \text{pM}$) it seems likely that typical binding affinities between substrates and their cognate receptors are even lower than 10nM. Substrate degradation has been modeled through a first order process of the form $\text{Cul1.SR1.S1} \rightarrow \text{Cul1.SR1}$ with an effective first order rate constant of $k_{deg} = 0.004 \text{s}^{-1}$ (corresponding to 0.24min^{-1}).

To conduct the simulations shown in Fig 6 we considered two substrates (S1 and S2) each binding to its cognate SR with the same set of default values for $k_{on} = 10^8 \text{M}^{-1}\text{s}^{-1}$, $k_{off} = 1 \text{s}^{-1}$ and $k_{deg} = 0.004 \text{s}^{-1}$. In addition, we included another substrate receptor species (SR3) which collectively accounts for auxiliary receptors that compete for access to Cul1, but for which no substrate is available. To this end, we added three reversible binding equilibria similar to those already depicted for SR1 and SR2 assuming for each of the reactions the same value for the ‘on’ and ‘off’ rate constants as for SR1 and SR2. To generate the curves in Fig 6A and 6D we lowered the k_{on} for S1 5-fold to $k_{on} = 2 \cdot 10^7 \text{M}^{-1}\text{s}^{-1}$ so that $K_{D,S1} = 5 \cdot K_{D,S2}$. To generate the curves in Fig 6B and 6E we increased $k_{sr,1}$ for SR1 5-fold to $k_{sr,1} = 4.5 \cdot 10^{-6} \text{s}^{-1}$ so that the Cul1-binding affinity of SR1 is 5-fold lower compared to that of SR2, i.e. $K_{sr,1} = 5 \cdot K_{sr,2}$. To preserve the detailed balance relation (Eq 1) for the cycle involving SR1 we also increased the value of $k'_{sr,1}$ 5-fold to $k'_{sr,1} = 6.5 \text{s}^{-1}$.

Estimation of k'_{ca} . The rate constants listed in Table 1 were measured for the particular substrate receptor Fbxw7 using a FRET-based assay [10]. The dissociation constants K_{sr} and K'_{sr} were directly computed from the reported values of the ‘on’ and ‘off’ rate constants. For the dissociation constant $K'_{ca} = \eta K'_{sr}$ an upper limit of 50nM has been reported. Using this value as an estimate for K'_{ca} yields $\eta \approx 0.077$. The remaining dissociation constant is then determined by the detailed balance relation (Eq 1) which yields $K_{ca} \approx 1.73 \cdot 10^{-5} \text{nM}$. From the 4 dissociation rate constants listed in Table 1 only k'_{ca} had not been measured. To estimate this parameter we repeat the experiment in Fig 4B from Ref. [10] in a computer simulation (Fig 8). Here, 70nM of CFP-tagged Cul1 was first incubated with 70nM β -TrCP-Skp1 which sequestered essentially all the available Cul1. Hence, subsequent addition of TAMRA-labelled Fbxw7 (Fbxw7^{TAMRA}-Skp1) did not evoke a change in donor fluorescence since Fbxw7-Skp1 could not gain access to Cul1. However, in the presence of 150nM Cand1 the fluorescence signal

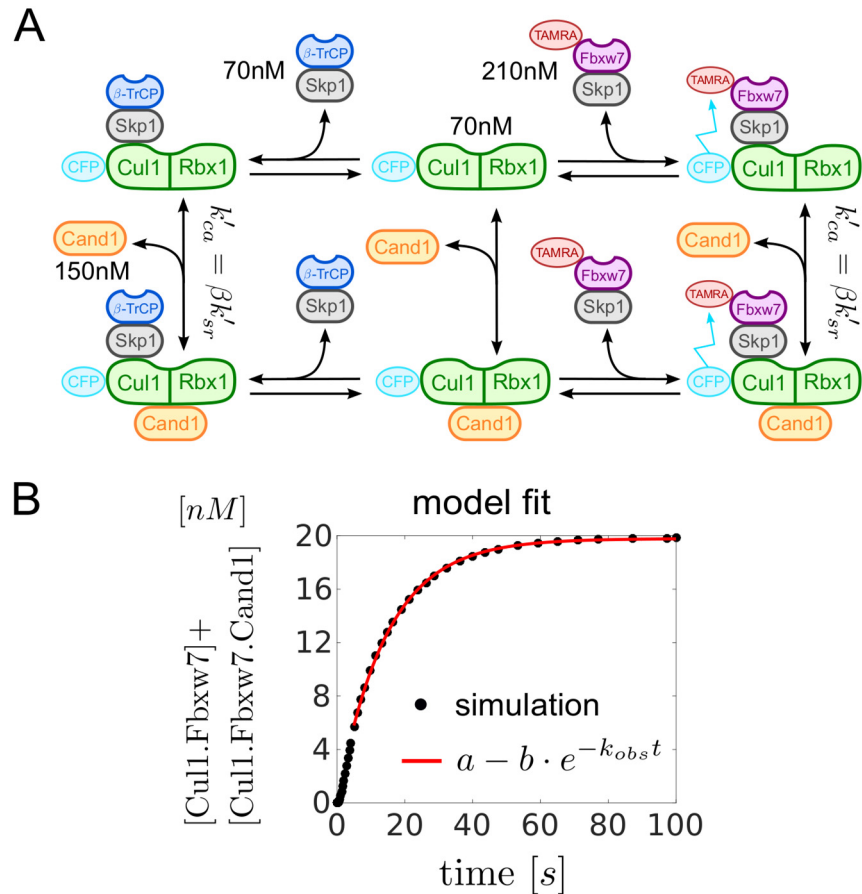


Fig 8. Estimation of $k'_{ca} = \beta k'_{sr}$. **A:** Scheme showing the reactions as used in the experimental setup of Pierce et al. [10]. States and reactions have the same meaning as in Fig 1B. Note that Cul1 and Fbxw7 are bound to fluorescent dyes. **B:** Fit of the model simulations to a single exponential function. Data points for the first 5 seconds were discarded to obtain a better fit. Kinetic parameters were taken from Table 1.

<https://doi.org/10.1371/journal.pcbi.1005869.g008>

decayed over time due to Cand1-mediated exchange of β -TrCP for Fbxw7. An exponential fit to the time course of the signal yielded a first order rate constant of $k_{obs} \approx 0.07s^{-1}$. In our model we have changed $k'_{ca} = \beta k'_{sr}$ (the only free parameter) until the time scale for reaching the steady state coincided with that observed experimentally (Fig 8B). As a result we obtained $k'_{ca} = 0.04s^{-1}$ or $\beta = 0.031$.

Supporting information

S1 Text. Steady state and time scale analysis of the Cand1 cycle model. In S1 Text we conduct a steady state / time scale analysis of Eq (3) and provide the derivations of Eqs (5)–(9). (PDF)

Acknowledgments

We thank Michal Sharon and Wolfgang Dubiel for comments on the manuscript. RS is grateful for discussions with Ray Deshaies. DF is deeply grateful for the support by the Max Planck Institute for Dynamics of Complex Technical Systems and for support by the Institute for Automation Engineering (IFAT) at the Otto-von-Guericke-University Magdeburg.

Author Contributions

Conceptualization: Ronny Straube, Dieter A. Wolf.

Formal analysis: Ronny Straube, Dietrich Flockerzi.

Funding acquisition: Dieter A. Wolf.

Investigation: Meera Shah.

Validation: Ronny Straube, Meera Shah, Dietrich Flockerzi, Dieter A. Wolf.

Writing – review & editing: Ronny Straube, Dietrich Flockerzi, Dieter A. Wolf.

References

1. Petroski MD, Deshaies RJ. Function and regulation of cullin-RING ubiquitin ligases. *Nat Rev Mol Cell Biol.* 2005; 6:9–20.
2. Kommander D, Rape M. The ubiquitin code. *Annu Rev Biochem.* 2012; 81:203–229. <https://doi.org/10.1146/annurev-biochem-060310-170328>
3. Wang Z, Liu P, Inuzuka H, Wei W. Roles of F-box proteins in cancer. *Nat Rev Cancer.* 2014; 14:233–247. <https://doi.org/10.1038/nrc3700> PMID: 24658274
4. Kitagawa K, Kitagawa M. The SCF-type E3 ubiquitin ligases as cancer targets. *Curr Cancer Drug Targets.* 2014; 16:119–129. <https://doi.org/10.2174/1568009616666151112122231>
5. Tikhmyanova N, Tutton S, Martin KA, Lu F, Kossenkov AV, Paparoidamis N, et al. Small molecule perturbation of the CAND1-CUL1-ubiquitin cycle stabilizes p53 and triggers Epstein-Barr virus reactivation. *PLoS Pathog.* 2017; 13:e1006517. <https://doi.org/10.1371/journal.ppat.1006517> PMID: 28715492
6. Skowrya D, Craig KL, Tyers M, Elledge SJ, Harper JW. F-box proteins are receptors that recruit phosphorylated substrates to the SCF ubiquitin-ligase complex. *Cell.* 1997; 91:209–219. [https://doi.org/10.1016/S0092-8674\(00\)80403-1](https://doi.org/10.1016/S0092-8674(00)80403-1) PMID: 9346238
7. Feldman RM, Correll CC, Kaplan KB, Deshaies RJ. A complex of Cdc4p, Skp1p, and Cdc53p/cullin catalyzes ubiquitination of the phosphorylated CDK inhibitor Sic1p. *Cell.* 1997; 91:221–230. [https://doi.org/10.1016/S0092-8674\(00\)80404-3](https://doi.org/10.1016/S0092-8674(00)80404-3) PMID: 9346239
8. Lydeard JR, Schulman BA, Harper JW. Building and remodelling cullin-RING E3 ubiquitin ligases. *EMBO Rep.* 2013; 14:1050–1061. <https://doi.org/10.1038/embor.2013.173> PMID: 24232186
9. Bennett EJ, Rush J, Gygi SP, Harper JW. Dynamics of cullin-RING ubiquitin ligase network revealed by systematic quantitative proteomics. *Cell.* 2010; 143:951–965. <https://doi.org/10.1016/j.cell.2010.11.017> PMID: 21145461
10. Pierce NW, Lee JE, Liu X, Sweredoski MJ, Graham RLJ, Larimore EA, et al. Cand1 promotes assembly of new SCF complexes through dynamic exchange of F box proteins. *Cell.* 2013; 153:206–215. <https://doi.org/10.1016/j.cell.2013.02.024> PMID: 23453757
11. Scott DC, Rhee DY, Duda DM, Kelsall IR, Olszewski JL, Paulo JA, et al. Two distinct types of E3 ligases work in unison to regulate substrate ubiquitylation. *Cell.* 2016; 166:1198–1214. <https://doi.org/10.1016/j.cell.2016.07.027> PMID: 27565346
12. Kawakami T, Chiba T, Suzuki T, Iwai K, Yamanaka K, Minato N, et al. NEDD8 recruits E2-ubiquitin to SCF E3 ligase. *EMBO J.* 2001; 20:4003–4012. <https://doi.org/10.1093/emboj/20.15.4003> PMID: 11483504
13. Duda DM, Borg LA, Scott DC, Hunt HW, Hammel M, Schulman BA. Structural insights into NEDD8 activation of cullin-RING ligases: Conformational control of conjugation. *Cell.* 2008; 134:995–1006. <https://doi.org/10.1016/j.cell.2008.07.022> PMID: 18805092
14. Saha A, Deshaies RJ. Multimodal activation of the ubiquitin ligase SCF by Nedd8 conjugation. *Mol Cell.* 2008; 32:21–31. <https://doi.org/10.1016/j.molcel.2008.08.021> PMID: 18851830
15. Lyapina S, Cope G, Shevchenko A, Serino G, Truge T, Zhou C, et al. Promotion of NEDD-CUL1 conjugate cleavage by COP9 signalosome. *Science.* 2001; 292:1382–1385. <https://doi.org/10.1126/science.1059780> PMID: 11337588
16. Cavidini S, Fischer ES, Bunker RD, Potenza A, Lingaraju GM, Goldie KN, et al. Cullin-RING ubiquitin E3 ligase regulation by the COP9 signalosome. *Nature.* 2016; 531:598–603. <https://doi.org/10.1038/nature17416>

17. Wu S, Zhu W, Nhan T, Toth JI, Petroski MD, Wolf DA. CAND1 controls *in vivo* dynamics of the cullin 1-RING ubiquitin ligase repertoire. *Nat Commun.* 2013; 4:1642. <https://doi.org/10.1038/ncomms2636> PMID: 23535663
18. Zemla A, Thomas Y, Kedzioro S, Knebel A, Wood NT, Rabut G, et al. CSN- and CAND1-dependent remodelling of the budding yeast SCF complex. *Nat Commun.* 2013; 4:1641. <https://doi.org/10.1038/ncomms2628> PMID: 23535662
19. Goody RS, Hofmann-Goody W. Exchange factors, effectors, GAPs and motor proteins: common thermodynamic and kinetic principles for different functions. *Eur Biophys J.* 2002; 31:268–274. <https://doi.org/10.1007/s00249-002-0225-3> PMID: 12122473
20. Zheng J, Yang X, Harrell JM, Ryzhikov S, Shim EH, Lykke-Andersen K, et al. CAND1 binds to unneddylated CUL1 and regulates the formation of SCF ubiquitin E3 ligase complex. *Mol Cell.* 2002; 10:1519–1526. [https://doi.org/10.1016/S1097-2765\(02\)00784-0](https://doi.org/10.1016/S1097-2765(02)00784-0) PMID: 12504026
21. Feng S, Shen Y, Sullivan JA, Rubio V, Xiong Y, Sun TP, et al. *Arabidopsis* CAND1, an unmodified CUL1-interacting protein is involved in multiple developmental pathways controlled by ubiquitin/proteasome-mediated protein degradation. *Plant Cell.* 2004; 16:1870–1882. <https://doi.org/10.1105/tpc.021949> PMID: 15208391
22. Chuang HW, Zhang W, Gray WM. *Arabidopsis* ETA2, an apparent ortholog of the human cullin-interacting protein CAND1, is required for auxin responses mediated by the SCF(TIR1) ubiquitin ligase. *Plant Cell.* 2004; 16:1883–1897. <https://doi.org/10.1105/tpc.021923> PMID: 15208392
23. Lo SC, Hannink M. CAND1-mediated substrate adaptor recycling is required for efficient repression of Nrf2 by Keap1. *Mol Cell Biol.* 2006; 26:1235–1244. <https://doi.org/10.1128/MCB.26.4.1235-1244.2006> PMID: 16449638
24. Schmidt MW, McQuary PR, Wee S, Hofmann K, Wolf DA. F-box-directed CRL complex assembly and regulation by the CSN and CAND1. *Mol Cell.* 2009; 35:586–597. <https://doi.org/10.1016/j.molcel.2009.07.024> PMID: 19748355
25. Bornstein G, Ganoth D, Hershko A. Regulation of neddylation and deneddylation of cullin1 in SCF^{Skp2} ubiquitin ligase by F-box protein and substrate. *Proc Natl Acad Sci USA.* 2006; 103:11515–11520. <https://doi.org/10.1073/pnas.0603921103> PMID: 16861300
26. Liu J, Furukawa M, Matsumoto T, Xiong Y. NEDD8 Modification of CUL1 dissociates p120^{CAND1}, an inhibitor of CUL1-SKP1 binding and SCF ligases. *Mol Cell.* 2002; 10:1511–1518.
27. Goldenberg SJ, Cascio TC, Shumway SD, Garbutt KC, Liu J, Xiong Y, et al. Structure of the Cand1-Cul1-Roc1 complex reveals regulatory mechanisms for the assembly of the multisubunit cullin-dependent ubiquitin ligases. *Cell.* 2004; 119:517–528. <https://doi.org/10.1016/j.cell.2004.10.019> PMID: 15537541
28. Siergiejuk E, Scott DC, Schulman BA, Hofmann K, Kurz T, Peter M. Cullin neddylation and substrate-adaptors counteract SCF inhibition by the CAND1-like protein Lag2 in *Saccharomyces cerevisiae*. *EMBO J.* 2009; 28:3845–3856. <https://doi.org/10.1038/emboj.2009.354> PMID: 19942853
29. Bai C, Sen P, Hofmann K, Ma L, Goebel M, Harper JW, et al. SKP1 connects cell cycle regulators to the ubiquitin proteolysis machinery through a novel motif, the F-box. *Cell.* 1996; 86:263–274. [https://doi.org/10.1016/S0092-8674\(00\)80098-7](https://doi.org/10.1016/S0092-8674(00)80098-7) PMID: 8706131
30. Emberly ED, Mosadeghi R, Deshaies RJ. Deconjugation of Nedd8 from Cul1 is directly regulated by Skp1-F-box and substrate, and the COP9 signalosome inhibits deneddylation of SCF by a noncatalytic mechanism. *J Biol Chem.* 2012; 287:29679–29689. <https://doi.org/10.1074/jbc.M112.352484>
31. Enchev RI, Scott DC, da Fonseca PCA, Schreiber A, Monda JK, Schulman BA, et al. Structural basis for a reciprocal regulation between SCF and CSN. *Cell Rep.* 2012; 2:616–627. <https://doi.org/10.1016/j.celrep.2012.08.019> PMID: 22959436
32. Kominami K, Ochotorena I, Toda T. Two F-box/WD-repeat proteins Pop1 and Pop2 form hetero- and homo-complexes together with cullin-1 in the fission yeast SCF (Skp1-Cullin-1-F-box) ubiquitin ligase. *Genes Cells.* 1998; 3:721–735. <https://doi.org/10.1046/j.1365-2443.1998.00225.x> PMID: 9990507
33. Wolf DA, McKeon F, Jackson PK. F-box/WD-repeat proteins Pop1p and Sud1p/Pop2p form complexes that bind and direct the proteolysis of Cdc18p. *Curr Biol.* 1999; 9:373–376. [https://doi.org/10.1016/S0960-9822\(99\)80165-1](https://doi.org/10.1016/S0960-9822(99)80165-1) PMID: 10209119
34. Jallepalli PV, Tien D, Kelly TJ. *sud1(+)* targets cyclin-dependent kinase-phosphorylated Cdc18 and Rum1 proteins for degradation and stops unwanted diploidization in fission yeast. *Proc Natl Acad Sci USA.* 1998; 95:8159–8164. <https://doi.org/10.1073/pnas.95.14.8159> PMID: 9653157
35. Seibert V, Prohl C, Schoultz I, Rhee E, Lopez R, Abderazzaq K, et al. Combinatorial diversity of fission yeast SCF ubiquitin ligases by homo- and heterooligomeric assemblies of the F-box proteins Pop1p and Pop2p. *BMC Biochem.* 2002; 3:22. <https://doi.org/10.1186/1471-2091-3-22> PMID: 12167173

36. Dubiel D, Ordermann J, Pratschke J, Dubiel W, Naumann M. CAND1 exchange factor promotes Keap1 integration into cullin 3-RING ubiquitin ligase during adipogenesis. *Int J Biochem Cell Biol.* 2015; 66:95–100. <https://doi.org/10.1016/j.biocel.2015.07.013> PMID: 26219975
37. Klebe C, Prinz H, Wittinghofer A, Goody RS. The kinetic mechanism of Ran-nucleotide exchange catalyzed by RCC1. *Biochem.* 1995; 34:12543–12552. <https://doi.org/10.1021/bi00039a008>
38. Gromadski KB, Wieden HJ, Rodnina MV. Kinetic mechanism of elongation factor Ts-catalyzed nucleotide exchange in elongation factor Tu. *Biochem.* 2002; 41:162–169. <https://doi.org/10.1021/bi015712w>
39. Wieden HJ, Mercier E, Gray J, Steed B, Yawney D. A combined molecular dynamics and rapid kinetics approach to identify conserved three-dimensional communication networks in elongation factor Tu. *Bio-phys J.* 2010; 99:3735–3743. <https://doi.org/10.1016/j.bpj.2010.10.013> PMID: 21112298
40. Goryachev AB, Pokhilko AV. Computational model explains high activity and rapid cycling of Rho GTPases within protein complexes. *PLoS Comp Biol.* 2006; 2:e172. <https://doi.org/10.1371/journal.pcbi.0020172>
41. Stanley RJ, Thomas GMH. Activation of G proteins by guanine nucleotide exchange factors relies on GTPase activity. *PLoS ONE.* 2016; 11:e0151861. <https://doi.org/10.1371/journal.pone.0151861> PMID: 26986850
42. Dhooge A, Govaerts W, Kuznetsov YA. MATCONT: A MATLAB package for numerical bifurcation analysis of ODEs. *ACM T Math Software.* 2003; 29:141–164. <https://doi.org/10.1145/779359.779362>
43. MATLAB 2015b. The MathWorks. Natick; 2015.